Calcification types of *Oocardium stratum* Nägeli and microhabitat conditions in springs of the Alps

Eugen Rott[1,5], Ralf Hotzy[2,6], Marco Cantonati[3,7], AND Diethard Sanders[4,8]

[1] *Institute of Botany, University of Innsbruck, Sternwartestrasse 15, 6020 Innsbruck, Austria*
[2] *Landesbund für Vogelschutz in Bayern, Eisvogelweg 1, 91161 Hilpoltstein, Germany*
[3] *Museo delle Scienze, Limnology and Phycology Section, Via Calepina 14, 38122 Trento, Italy*
[4] *Institute of Geology and Paleontology, University of Innsbruck, Innrain 52, 6020 Innsbruck, Austria*

Abstract. Habitat conditions and spring-associated limestones (SALs) formed by ambient precipitation with the biotic contribution of the desmid *Oocardium stratum* Nägeli 1843 (Zygnematophyceae) were studied in 5 springs along a north–south transect across the central Eastern European Alps. Spring waters were characterized by permanent flow and temporally almost stable physicochemical conditions, but variable relationships among major ions (especially HCO_3^-:SO_4^{2-} and Ca^{2+}:Mg^{2+}) among sites. In most cases, CO_2 supersaturation (0.2–1.8 µM/L) caused in situ depression of pH from near equilibrium (8.3) to <8, with a minimum pH of 7.1. SAL areas dominated by *Oocardium* growth were greatest some distance downstream of the spring origin where degassing of excess CO_2 had occurred and pH had risen to >8.1. The calcified segments of spring streams were limited to areas <300 m from the spring mouth. Within the uppermost segment of larger rheocrenes (CO_2 supersaturated areas), extensive weakly calcified bryophyte crops (*Eucladium verticillatum*, *Palustriella commutata*) were replaced further downstream by *Oocardium*-spiked calcified coatings. The various morphologies of *Oocardium* cells (assessed with light microscopy [LM], scanning electron microscopy [SEM], and petrographic thin sections) revealed different types of calcification, from micritic (<1–4 µm) to sparitic calcites (>100–1000 µm) whose ultrastructural features were best seen with SEM. The distribution of SAL types within and among sites was evaluated in relation to water-chemistry and additional environmental variables. The findings were compared with earlier records from the Alps and other mountain areas of Europe (in particular, Croatia and UK) to facilitate recognition and delimitation of *Oocardium* niches in the environment and to foster protection of these rare habitats.

Key words: biocalcification, *Oocardium* calcification signature, habitat niche, cool springs, calcite, desmids, freshwater, in situ pH, in situ free CO_2.

Cool calcareous springs (nonthermal, <20°C at emergence) provide natural laboratories to study biocalcification. The physicochemical conditions of spring waters are modified during percolation through aquifers and soils by abiotic reactions with the lithosphere and nonphotosynthetic microbial processes. On appropriate bedrocks, these modifications lead to nonequilibrium water-chemistry conditions (supersaturation of dissolved salts and gases, especially CO_2). From the point of entry of the water to the atmosphere, degassing and subsequent precipitation of excess dissolved salts occur until equilibri-

um with the partial pressure of CO_2 in the atmosphere is reached (Hütter 1994). This process can cause spatially delimited mineral deposition modified and intensified by sessile benthic organisms to reach deposition rates of >1 mm/mo (Sanders and Rott 2009).

Biotic influence on calcification in springs can be essential, but the taxon-specific role of organisms in spring-associated limestone (SAL) formation tends to be underestimated (Golubić et al. 2008). Biogenic calcification products of algae and cyanobacteria in lotic freshwaters range from soft micritic oncoids formed by trapping, binding, cementation, and decomposition processes (algal micro-reefs, sensu Schneider et al. 1983; Rott 1991) to solid sparitic deposits, of which calcified *Rivularia* spp. (Cyanobacteria) is a well known example (Pentecost 1987,

Obenlüneschloss and Schneider 1991). In alpine cool SALs, calcifying cyanobacteria seem to be most common. In a study by Cantonati et al. (2012), the cyanobacteria *Phormidium incrustatum* (Nägeli) Gomont ex Gomont and *Tapinothrix crustacea* (Voronichin) Komárek were the dominant calcifiers in SALs (5 of 6 cases), whereas *Oocardium stratum* was only found in 1 spring.

Calcification of the filamentous algae varies from direct apposition to cell walls to calcification of the outer cell wall (mucilage) layers, but *Oocardium* coenobia consisting of loosely associated single cells or pairs of cells are characterized by primarily noncalcified tubular structures and later calcification distant from the cell wall (Wallner 1933, 1935, Golubić et al. 2008). The cells are held in an oblique position within mucilage tubes secreted through multiple cell-wall pores arranged around a single apical master pore (Rott et al. 2010), apparently hindering direct calcification of the cell wall.

In the central part of the Eastern European Alps, springs with SAL were recorded over a wide altitudinal range (up to 2500 m asl) (Sanders et al. 2010). Little is known about the variability of spring-related calcification by specific organisms, but biocalcification imprints vary from exclusively inorganic precipitates (especially for calcites) to specific signatures of organic structures generating particular mineralogical products. Unfortunately, Alpine spring capture for drinking water, artificial snow, and micro-electric power generation causes rapid degradation of these springs (Cantonati et al. 2009). Degradation of numerous sites in Bavaria from which *Oocardium* had been recorded in the 1930s (Wallner 1934a, b) was observed recently (ER, personal observation). The only spring type protected by the European Habitat Directive (EU HD 1992), those with SALs, may be overlooked even by experts because their calcifiers (*Oocardium stratum* cells ≈ 20 μm, barely visible with a hand lens) are minute and scarce at times of low flow or in winter, when overgrown by other algae (Sanders and Rott 2009).

The number of recent studies of *Oocardium* from Europe with detailed structural and ultrastructural data is low (Pentecost 1991, Golubić et al. 1993, 2008), but *Oocardium* has been recorded from temperate and tropical latitudes on other continents (Cuba, Rieth 1970; Oklahoma, Pentecost 1991). Details of *Oocardium* deposystems geology, calcification, and ultrastructure have been studied recently at 2 sites in the Austrian Alps (Sanders and Rott 2009, Rott et al. 2010). A more extended study of the calcite ultrastructure, with additional information on the physicochemical conditions of the habitat should provide better insights into the response of *Oocardium* to the environment. We hypothesize that environmental factors, particularly water chemistry at the spring mouth, will be related to the type (style) of initial calcification and the quality of the final calcite deposition type.

Methods

Geographical and geological description of sites

The Hochtalalm spring (H in Fig. 1) lies in the Weissach Valley, a western tributary of the Brandenberger Ache in northern Tyrol within an extended mixed forest interspersed by open pastures. The spring emerges from carbonate rocks (Wetterstein Limestone) on a steep east-facing mountain flank. The Wetterstein Limestone is a thick succession of partly dolomitized shallow-water limestones that underlies the entire topographic recharge area of the spring. Only the eastern side branch of the seepage area from ~8 m downstream of its bryophyte-covered emergence is calcified. SALs are found along the whole stream course, over a sequence of steep cascades and shallower pool and riffle areas.

The Lingenau spring (L) is part of an extended zone of active and fossil SAL in Bregenzerwald (Vorarlberg, Austria). We focused on the permanent spring-brook in the western part of the spring area. A few meters downstream of its emergence, the water cascades over a waterfall, then follows an inclined reach with SAL pools, rimstones, and shelfstones, finally falling down a 2nd waterfall into the gorge of the River Subersach. The geographic position is on the southwestern margin of a plateau that falls ~80 m to the river gorge. The active SAL deposit is situated above a truncated succession of shallow marine conglomerates, marls, and sandstones (Weissach Formation; Upper Oligocene) veneered by glacial lodgement till and proglacial fluvial deposits (for details see Sanders and Rott 2009).

The Paterzell spring (P) originates in the center of a large yew grove in a protected forest in Bavaria (Germany) situated on the eastern slope of hills delimiting the Ammer valley to the west. The spring emerges from an erosional remnant of a proglacial veneer of gravels and sands ascribed to the Mindel glaciation. However, for most of its extent, the spring is surrounded by glacial till and proglacial deposits (gravels, sands, clays) of the Würmian glaciation. Estimating the extent of the recharge area and the percolation path of the spring is difficult because of a gentle northward gradient. The spring water, or some of it, might stem from percolation through deposits of the underlying Molasse Zone (sand, clay, gravel), which are exposed ~5–10 km to the south. Vivid
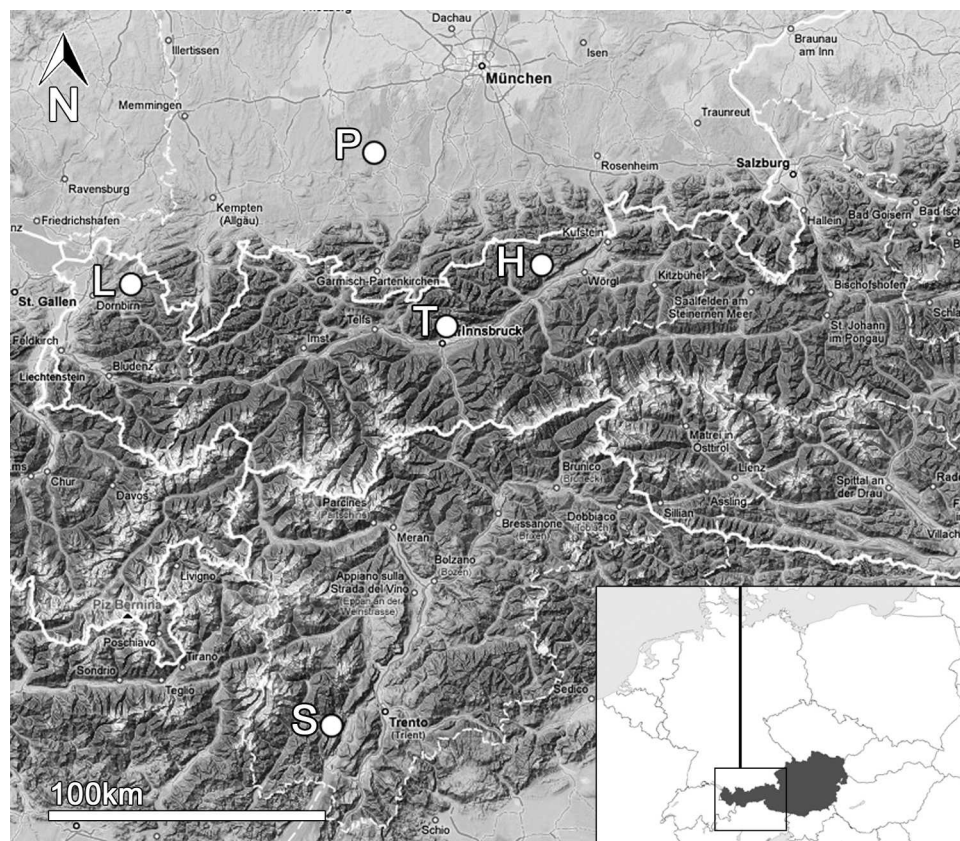
FIG. 1. Geographic position of sampling sites within a cross section of the central eastern Alps between Germany to the North and Italy to the south. H = Hochtalalm, L = Lingenau, P = Paterzell, S = Spiazzi, T = Tuffbach.

green *Oocardium* cover was found only in the seepage areas close to the highway crossing the forest and on riffles in the adjacent spring stream (~30 L/s) over ~150 m.

Spiazzi spring (S) near Ponte Arche in the Sarca valley (Trentino, Italy) is a minute permanent spring at the eastern end of a wider seepage area on a gravel slope. A narrow flow of water drops over calcified mosses at the origin. The spring emerges from Paleogene neritic limestones and marls that probably determine much or all of the water chemistry. A contribution of groundwater percolating from higher parts of the recharge area, mainly Mesozoic limestones, cannot be excluded. A pollution effect is likely because the spring occurs within a settlement.

The Tuffbach spring (T), situated east of the Alpenzoo animal park near Innsbruck, originates as an isolated springbrook. The spring emerges from the lowest part of a south-dipping mountain flank composed mainly of Triassic carbonate rocks, just below the base of the Hötting Breccia (a lithified alluvial-fan succession) (for details see Sanders and Rott 2009). It forms a braiding area 15 m downstream of its origin where the water flows over a system of steps and pools built of moss-tufa terraces for another 30 m. Downstream of the moss tufa, an open canopied, narrower stream segment (30–40 m long) with a high proportion of *Oocardium* calcite is found, occasionally with *Rivularia* sp. as a secondary calcifier. The stream flows into a narrowing channel flowing through darker forested areas where *Oocardium* calcite disappears.

Sampling

Samples of water and calcite covered with calcified algae were taken ≥ 2 times from each spring. Water samples were collected in glass bottles from 3 stations (the spring mouth, the central *Oocardium* deposition zone, and the lower limit of calcification). Samples for morphological studies were taken from the permanently wetted perimeter of the reaches, from pebbles, wooden sticks, phytoclastics (incrusted fallen leaves and other dead plant material), and moss. A $10\times$ hand lens was used to select well developed macroscopic colonies if these were not visible to the naked eye. All samples were stored in a cool box before laboratory analysis.

TABLE 1.   Geography, geology, and characters of the deposystem of the 5 tufa springs (H = Hochtalalm, L = Lingenau, P = Paterzell, S = Spiazzi, T = Tuffbach).

Variable	Site H1	Site L1	Site P1	Site S1	Site T1
Longitude (E)	11°53′16″	9°54′29″	11°02′57″	10°52′00″	11°23′59″
Latitude (N)	47°32′57″	47°26′34″	47°51′30″	46°02′08″	47°17′04″
Altitude (m asl)	880	600	650	400	750
Exposition	E	SW	NE	NW	SE
Geology	Middle Triassic carbonate rocks	Paleogene conglomerates, sands, and marls	Proglacial deposits of Würmian glaciation	Paleogene limestones and marls	Triassic dolostones, limestones, and cellular dolomites
Aquifer	As above	Proglacial gravels and sands	Proglacial gravels and sands of Mindel glacial	As above	Lithified Quarternary alluvial-fan succession
Deposystem	Hillslope-paludal origin and cascading basin on steep slope/ waterfall	Extended waterfall tufa system	Gentle slope percolating system covered by wetland *Taxus* forest	Steep slope seepaging zone	Single spring, moss-tufa terraces and cascading channel
Oocardium area/ zone	Restricted to middle cascade part starting close to origin	Extended over large exposed terraces	Restricted to permanently flowing areas of small creeks	Restricted to permanently percolated areas	Restricted zone between moss terraces and dense forest

Water chemistry and laboratory methods

In situ measurements were made with a LF 91 conductimeter (conductivity and temperature; WTW, Weilheim, Germany) and a SevenGo pH-meter equipped with Inlab-Pure-Pro probe (pH and temperature; Mettler Toledo, Greifensee, Switzerland). Labile dissolved CO_2 gas (causing a pH shift to values of pH <7.5) was analyzed from samples kept in airtight Winkler glass bottles by back-titration to pH 8.2 (minus *p*-value) with 0.05 (or 0.1) N NaOH and then to pH 4.3 (*m*-value) with 0.1 N HCl in the field or immediately on return to the laboratory (samples were always kept as close as possible to, or below, in situ temperature to hinder CO_2 loss). In the field, glass field burettes, a magnetic stirrer (battery driven), and direct reading of the titration curve during the titration process were used. Triplicate samples were analyzed. The excess free CO_2 was calculated from CO_2 acidity (see Mackereth et al. 1978, Hütter 1994) assuming that CO_2 supersaturation of spring samples from the ground causes a reduction in pH (Hütter 1994).

Ion balance and related physicochemical conditions were analyzed at room temperature. SO_4^{2-} and major cation analyses followed standard methods of ion-exchange chromatography (Dionex; Vienna, Austria)

TABLE 2.   Water-chemistry conditions from the spring mouth in November 2010 (H, L, P, T) and August 2010 (S). Note the different units for major ions (mM/L) and nutrients (µg/L). See Fig. 1 for site abbreviations. n.a. = not available.

Sampling station	H1	L1	P1	S1	T1
Distance from origin (m)	5.0	0	0	0.2	0
T (°C)	10.6	10.9	10.7	13.3	8.7
pH$_{in\ situ}$	7.50	7.21	7.83	8.16	7.33
Conductivity (µS/cm$_{25°}$)	579	630	692	n.a.	1016
Ca^{2+} (mM/L)	4.53	6.21	5.39	3.44	7.52
Mg^{2+} (mM/L)	2.07	0.36	2.12	1.36	4.17
K^+ (mM/L)	0.02	0.12	0.03	0.05	0.03
Na^+ (mM/L)	0.02	0.23	0.22	0.35	0.11
HCO_3^- (mM/L)	6.47	6.14	6.79	4.28	3.72
CO_2 (mM/L)	0.47	1.85	1.14	0.16	1.19
Cl^- (mM/L)	0.03	0.30	0.17	0.25	0.11
SO_4^{2-} (mM/L)	0.02	0.17	0.18	0.38	7.76
Total P (PO_4-P µg/L)	7.7	1.8	2.4	0.9	2.7
NO_3-N (µg/L)	371	2694	2689	4012	859

TABLE 3. Variation of water-chemistry conditions from spring mouth (*Oocardium* maximum downstream) in summer (2 springs) and autumn (4 springs). L was sampled twice in autumn. See Fig. 1 for site codes.

Sampling station	H1–H2	H1–H2	L1–L2	L1–L2	P1–P2	P1–P2	T1–T2
Date	August 2010	November 2010	October 2008	November 2010	July 2010	November 2010	November 2010
Distance from origin (m)	5–80	5–80	0–50	0–50	0–150	0–150	0–80
T ($°C$)	10.6–12.0	8.9–8.3	7.2–8.1	10.8–10.1	10.7–11.5	10.4–9.2	8.7–9.6
$pH_{in\ situ}$	7.50–8.44	7.70–8.48	7.60–8.10	7.10–8.15	7.83–8.24	7.91–8.14	7.33–8.19
$Conductivity_{in\ situ}$ ($µS/cm$)	511–450	544–440	593–565	587–518	616–585	648–578	931–906
Ca^{2+} (mM/L)	4.04–3.51	4.53–4.62	6.20–5.92	6.21–4.72	5.18–4.82	5.39–4.63	7.52–7.23
Mg^{2+} (mM/L)	1.88–1.67	2.07–1.72	0.36–0.35	0.34–0.34	2.16–2.11	2.12–1.89	4.17–4.19
HCO_3^- (mM/L)	5.94–5.19	6.47–6.22	6.08–4.13	6.14–3.94	6.5–6.11	6.79–5.96	3.57–3.33
SO_4^{2-} (mM/L)	0.01–0.02	0.02–0.02	0.22–0.33	0.17–0.16	0.15–0.15	0.18–0.17	7.78–7.77

from gradually diluted samples (P. Franzoi, University of Innsbruck). NO_3^- was analyzed by ion chromatography (detection limit = 5 µg/L), and total P (TP) was analyzed with ammonium molybdate detection after treatment with sulfuric acid (detection limit = 0.5 µg/L).

Statistics

Features of the calcite and their relationship to environmental factors were tested using *t*-tests, Mann–Whitney *U*-tests, and analyses of variance (ANOVA) with Bonferroni correction. Log(*x*)-transformation in combination with nonparametric Mann–Whitney *U*-tests (Mann and Whitney 1947) gave the most reliable results because of the low number of replicates compared to the high number of environmental factors.

Light microscopy

Algal morphology was studied under a M3Z stereomicroscope (Wild, Heerbrugg, Switzerland) at 40× magnification. We used a Dialux M20 (Leitz, Wetzlar, Germany) equipped with 40×, 63×, and 100× objective lenses and a modified 7.2 electronic camera (Sony, Tokyo, Japan) for light microscopy (LM) images. LM measurements were taken with a calibrated eyepiece. Fresh algal material (tubular mucilage structure) was studied from hand-cut thin sections after gentle dissolution of the calcite in 0.2 N HCl. Mucilage tubes were stained with methylene-blue dissolved in aqueous ethanol.

Scanning electron microscopy (SEM)

For SEM investigation, washed *Oocardium* cells were gradually dehydrated in ethanol (from 10% to 99.5% in 10% steps; 30 min each) and transferred into formaldehyde-dimethyl-acetal (FDA, dimethoxymethane; Merck 8.06017.1000, Hohenbrunn, Germany) (Gerstberger and Leins 1978, Tschaikner et al. 2008) for 24 h followed by another addition for 2 h. To determine cell position within the calcite, critical-point (CP) drying was done with liquid CO_2 and FDA (our facilities did not allow the use of another gas). Both CP samples and untreated (nonCP) samples were sputter-coated with Au–Pd and examined with an XL20 SEM microscope (Philips, Eindhoven, The Netherlands).

Geological field assessments and mineralogy

SAL field activities consisted of mapping the entire deposystem at a scale of 1/2000 and sampling facies types for cut slabs and thin sections. Dried samples of active SAL were hardened with epoxy resin, cut, and
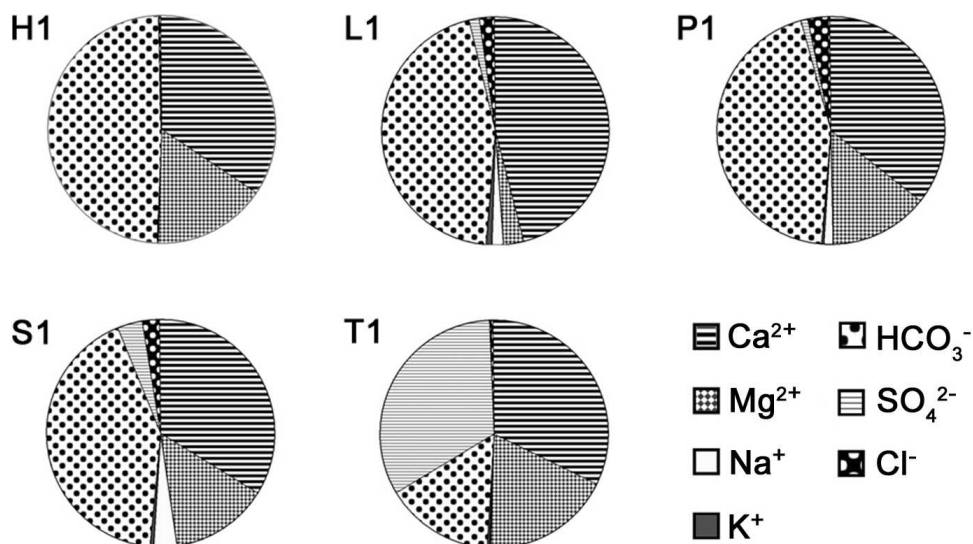
FIG. 2. Relative proportions of major ions in spring water from origins of the 5 springs. H = Hochtalalm, L = Lingenau, P = Paterzell, S = Spiazzi, T = Tuffbach.

slabbed. Petrographic thin sections (25 μm and 50 μm thick) of selected samples were investigated by polarized LM and dark-field microscopy. Diffraction patterns of powdered mineral samples were analyzed with standard x-ray diffraction (XRD) and with a parallel-beam technique to eliminate the effects of different heights of XRD powder samples and to determine Mg content by Rietveld refinement.

Details of the polarized LM and the explanation of the term crossed nicols.—In the microscope, thin sections of birefringent minerals can be viewed in polarized light with a uniform direction of vibration. The uniform direction of light vibration (= polarization of light) is produced by a lens called *polarizer*. In a birefringent mineral (or crystal), light rays passing through the mineral are split into an ordinary and extraordinary ray, with their vibration directions normal to each other (except if the light passes along a single preferred direction, the optical axis, which is relatively rarely encountered in thin section). In addition, upon passage of the mineral, the vibration direction of both the ordinary and the extraordinary ray is rotated relative to that of the initial polarization. After the light has passed the mineral and split into an ordinary and extraordinary ray, the light rays then must pass another polarization lens called the *analyzer*. In the analyzer, only light with a vibration direction normal to that of the first polarizer lens can pass. However, in a birefringent mineral, some light remains that can also pass the analyzer lens because of the splitting of light rays when passing the mineral. In the vast majority of cases, minerals are not oriented perfectly with their optical axis relative to the plane of thin section, but are oblique to it. As a result, in

a birefringent mineral, such as calcite (which has a single optical axis), 4 positions exist under the microscope where: 1) maximum light transmittance is possible (the crystal is well visible), and 2) no light transmittance through the analyzer lens is possible (the crystal turns black because of complete extinction of light). Thus, inspection of thin sections of mineral aggregates in a polarization microscope enables one to identify the size of individual crystals.

Terminology

The terms tufa or spring tufa to designate limestones formed from cool springs can be misleading for 2 reasons. First, without further qualification, tufa implies volcanic deposits or merely a highly macro- to megaporous rock (see Pedley 2009 for a history of the word tufa). Second, the diagnostic feature of spring tufa sensu stricto is high macro- to megaporosity, typically >10 to 15% (cf. Ford and Pedley 1996, Pentecost 2005). However, many spring limestones, not only hot-spring travertines, are low-porous and indurated. For such limestones, the term spring tufa is inappropriate. Therefore, we use the neutral term spring-associated limestones (SAL) for all types of limestones with low- to high-porosity deposited from hot or cold springs (see Sanders et al. 2010 for discussion).

Results

Comparison of the sites

The 5 sites are arranged along a rhombic cross-section of the central Eastern Alps, ~200 km north to
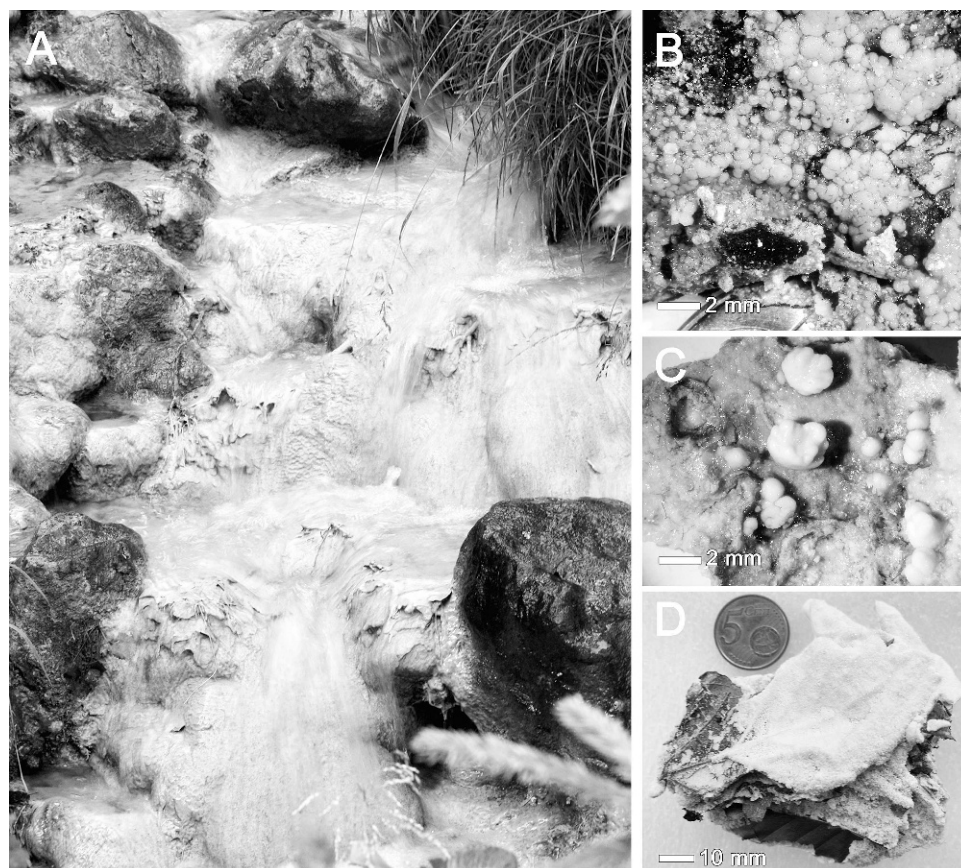
Fig. 3. Field aspect of a calcified stream segment (Hochtalalm 2) (A) and macroscopic aspects of *Oocardium* calcifications including small granular growth (scanning electron microscope [SEM] type 2) from Hochtalalm 1 (B), specific tooth-shaped growth from Spiazzi (C), and homogenous coating (SEM type 3) from Lingenau 2 (D).

south and 130 km east to west (Fig. 1), within an altitudinal range of 400 to 880 m asl (Table 1). Four sites lie within the Alps, and 1 is in the northern periAlpine area. The areas covered by *Oocardium* vary between a few m^2 (S) and >500 m^2 (L).

The waters from all 5 springs were characterized by temperatures related to mean air temperature and by moderate conductivity and buffering capacity (Table 2). pH measured in situ was depressed by acidification from excess dissolved CO_2 (0.2–1.8 μM/L) at 4 of the springs (Table 3). In all cases Ca^{2+} was the major cation, followed by Mg^{2+} with highly variable contribution to the ion balance between sites (Fig. 2). HCO_3^- was the dominant anion except at the Tuffbach, where SO_4^{2-} was 2× greater than HCO_3^- (gypsum layers in the catchment; Fig. 2; Table 2). TP (both inorganic and organic) was very low in all cases (<10 μg/L, but mostly <3 μg/L) indicating ultraoligotrophic conditions. On the other hand, NO_3^- was high in 3 springs (>2000 μg/L), which would be classified as N-eutrophic to N-hypertrophic (Wetzel 1975). NO_3^- enrichment was

related to extensive, repeatedly manured (spring and autumn), pasture land in the catchment.

Water-chemistry changed from the spring mouth along the stream areas toward the actively growing *Oocardium* zones (Table 3), with contrasting gradients of increasing pH (via CO_2 outgassing and periphyton photosynthesis) and decreasing conductivity (via calcification and concomitant reduction of dominant major ions, Ca^{2+}, HCO_3^-) along the stream.

Field aspects

Active to low-active spring-limestone deposition was found in all streams (Sanders et al. 2010). The lower reach of H, e.g., had large quantities of phytoclasts (leaves and pieces of wood), bryophytes and rock surfaces all covered by SAL across the wetted perimeter (Fig. 3A). Granular calcifications (<1 mm) were common in H (upper reach), P, and T. (Fig. 3B). Small tooth-like calcifications, similar to those from S (Fig. 3C) were also found in fast-flowing
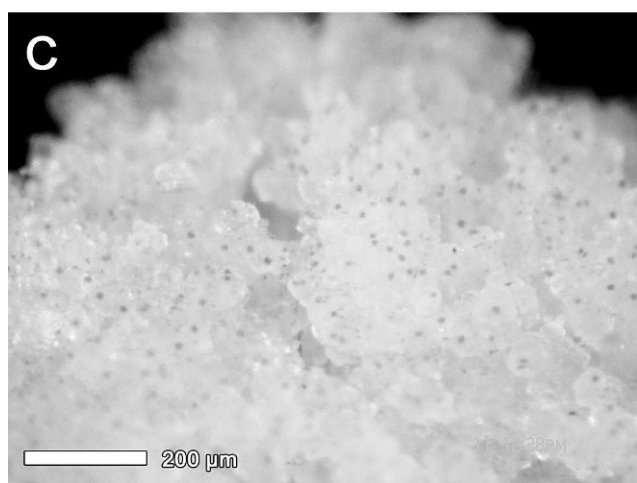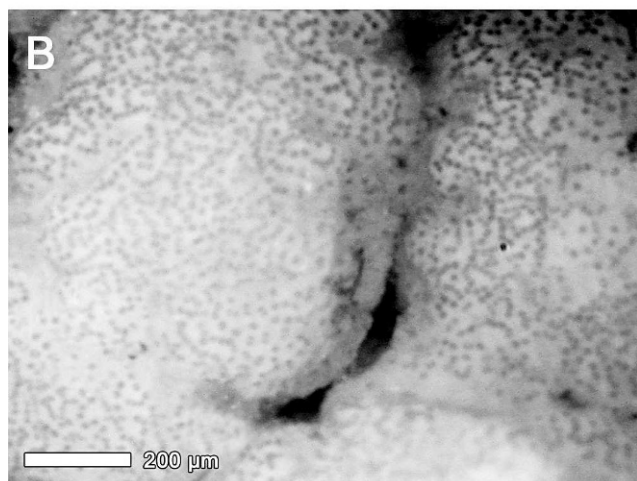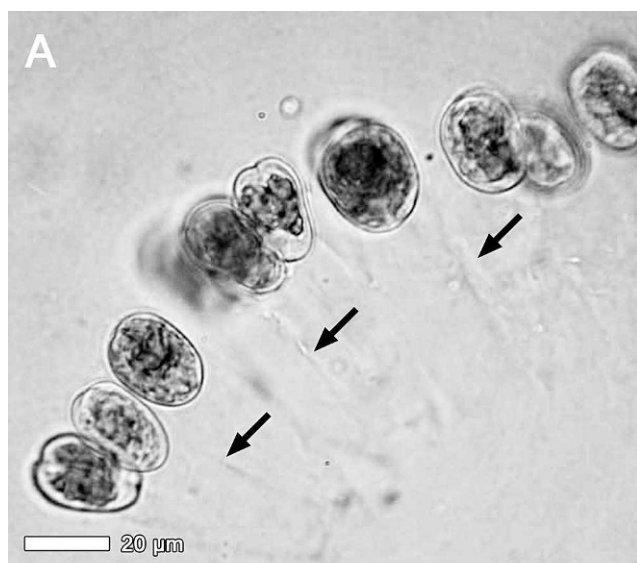
TABLE 4. *Oocardium* cell densities related to calcite features and referenced to figures in text. Calcite types: 1 = crystallites < 1 μm, 2 = crystallites > 1 to < 10 μm, 3 = orthospar crystals > 10 μm. n.s. = not shown.

Site	Date	Calcite type	Cells/mm²	Figure
H1	10 July 2010	2	1743	n.s.
H2	10 July 2010	3	1372	10A
L2	1 December 2007	3	385	4C
L2	24 October 2008	3	416	n.s.
P2	24 July 2009	1	1793	5A
P2	24 July 2009	1	2400	n.s.
P2	28 July 2010	1	920	n.s.
S1A	7 August 2009	1	2100	12B
S1B	7 August 2009	1	1290	12C
S1	11 July 2010	1	1590	n.s.
S1	11 July 2010	1	2487	n.s.
T2	13 April 2008	1	1320	n.s.
T2	11 August 2008	2	1320	n.s.
T2	11 August 2008	2	1650	4B

microhabitats at H. In H and L, calcification was most visible in late autumn and winter, when active *O. stratum* cells were sparse or absent. *Oocardium* calcite was visible as light-yellow to ochre limestone crusts with a sugar-like surface as is shown for a calcified leaf template from L (Fig. 3D). Surfaces rich in active *Oocardium* cells (spring and summer) usually had a distinct, light-green hue superimposed on the yellow surface of the calcite, but were dark green in riffle areas of P.

Calcification under LM

After gentle dissolution of calcites and methylene-blue staining (Fig. 4A), the typical cell outline is visible, i.e., drop-like or heart-shaped from the narrow lateral side (white arrows in Fig. 4A). The apex is situated on the broader lateral side so that the main cell axis is at right angles to the tubular mucilage fixing the cells within the calcite (see Golubić and Marcenko 1958). The density of the cells varied (Table 4, Fig. 4B, C), with minor changes in cell size (Rott et al. 2010). At higher magnification, 2 major styles of growth and calcification were visible: cauliflower-like with densely packed cells (Fig. 4B) and dendritic with more loosely packed cells (Fig. 4C). Macroscopically, the former appeared as a green flush on top of the white precipitate, whereas the dendritic type appeared as a very light green hue on the shiny yellow to brownish surface with scattered green spots (Fig. 4C).

FIG. 4. *Oocardium* light micrograph (LM) aspects including cell shape (white arrows: lateral views) and mucilage stalks (black arrows) in acid methylene-blue staining (A), cauliflower type growth form (scanning electron microscope

←

[SEM] type 1) from Tuffbach (B), and crystalline dendritic growth (SEM type 2) from Lingenau 2 (C).
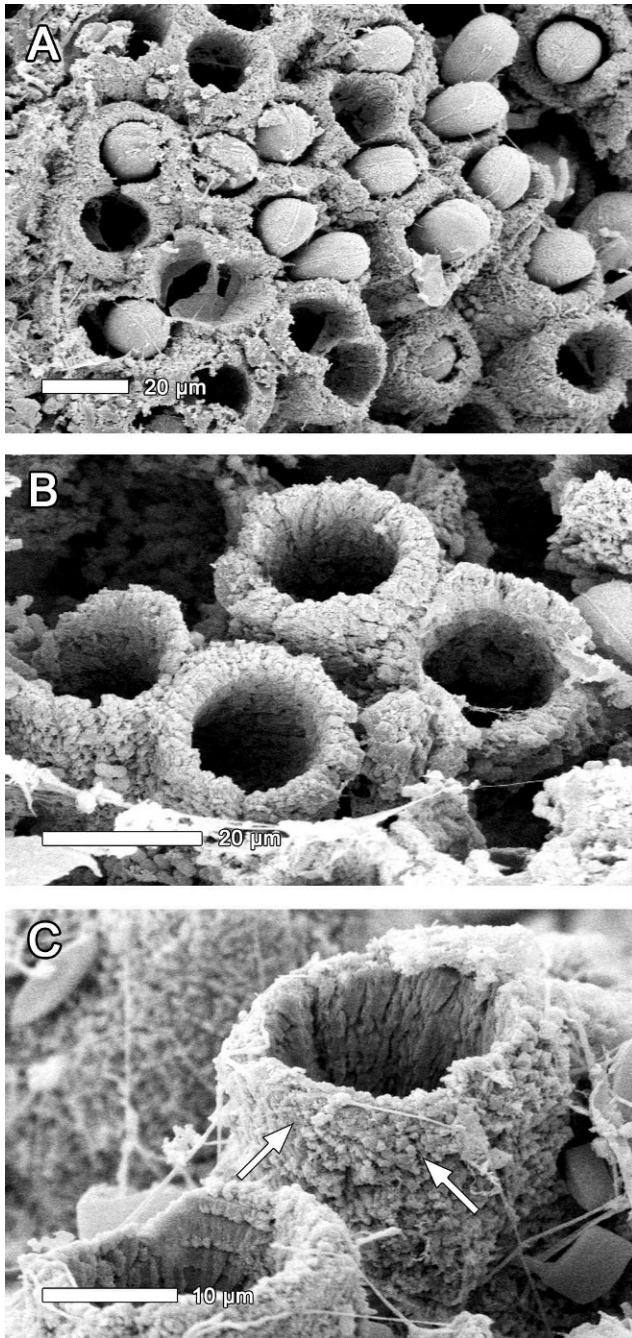
FIG. 5. Paterzell *Oocardium* calcification type 1 external aspects obtained with critical-point drying and scanning electron microscopy (CP SEM) showing conserved cell structures (A) and nonCP SEM of micritic extracellular calcite remains (B, C). Arrows in C point to granular (micritic) calcification from one cell.

Calcification types in SEM and petrographic thin sections

Calcification type 1.—At P, the initial calcification consisted of micritic crystallites, mostly <1 μm in size, of low-magnesian calcite (containing <4 mol % Mg in
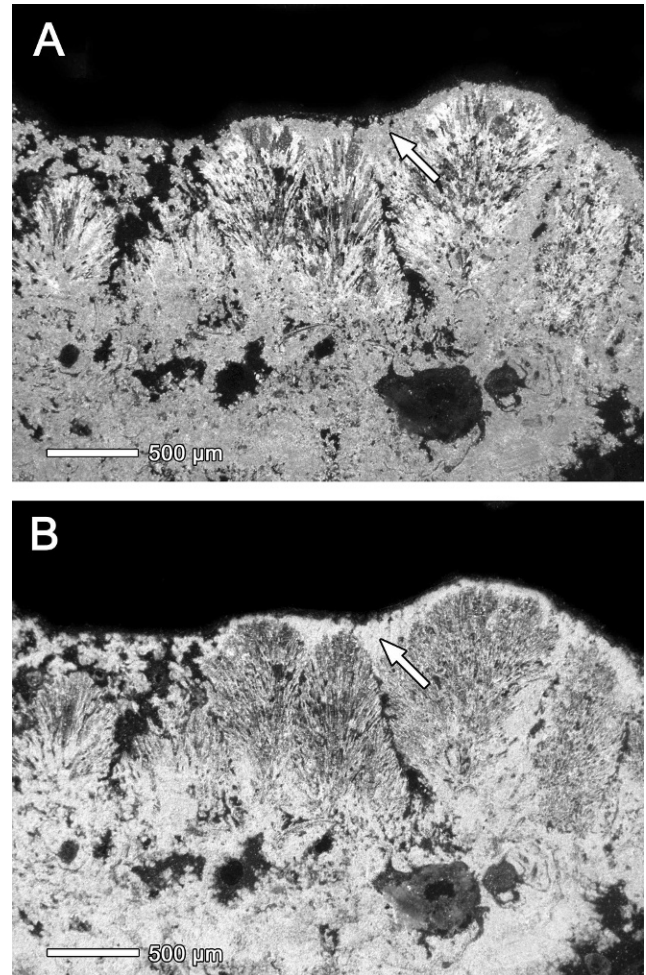

FIG. 6. Paterzell calcification type 1 petrographic cross sections in polarized light with dark field (A) and bright illumination (B). Arrows indicate primary crystallization (see text).

lattice) (Fig. 5A–C). This structure was best seen after removal of the organic cell contents (nonCP SEM; Fig. 5B, C). Because of the small size and poorly defined crystallographic surfaces of the crystallites, a preferred orientation with respect to upward growth of *O. stratum* could not be identified. In petrographic thin section, the initial calcification as numerous crystallites was shown by the grey lamina at the top (arrows in Fig. 6A, B). Sparitic *Oocardium* calcite with its typical radially fanning to arborescent structure (resulting from upward growth of *Oocardium* cells) was present under the micritic lamina (Fig. 6A, B; in B crossed nicols). Whether the micritic type of initial calcification recrystallizes diagenetically over time to generate the typical coarse-sparry *Oocardium* calcite is uncertain. This site is the first where micritic initial crystallization has been observed.
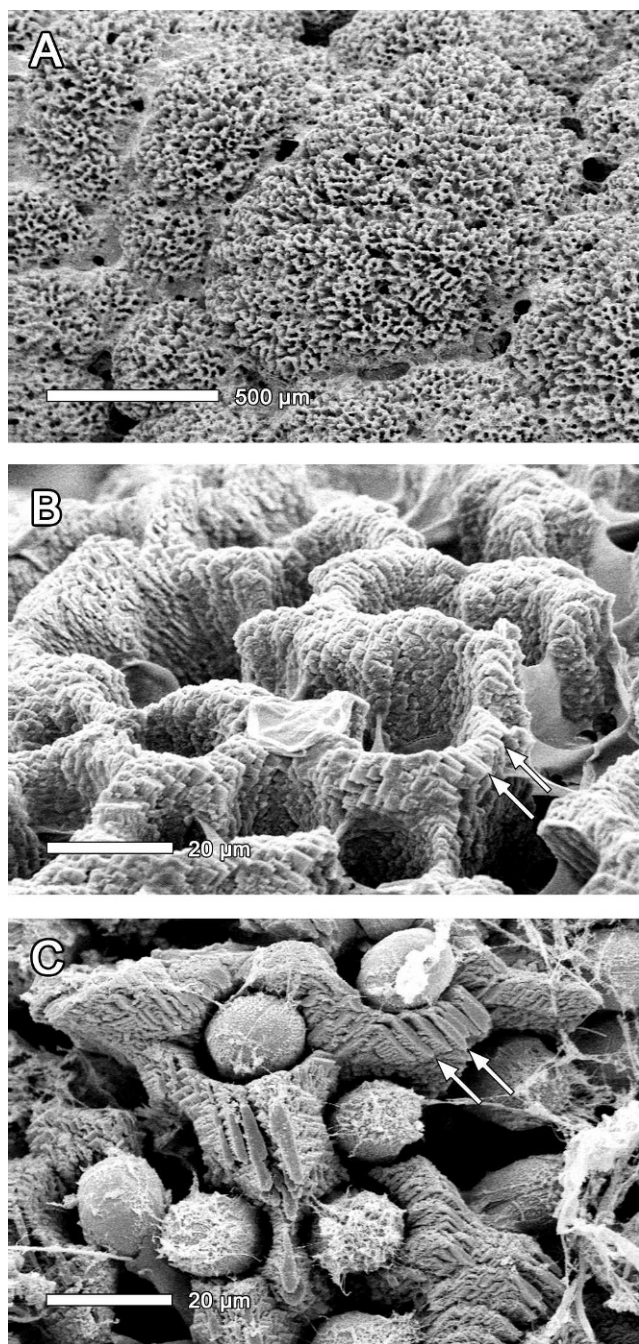
FIG. 7. Hochtalalm calcification type 2 shown with noncritical-point drying and scanning electron microscope (nonCP SEM) (A, B) and CP SEM (C). Arrows in B and C indicate examples of micro-rhombohedra as shown in Fig. 8A.

Calcification type 2.—At H1 (in the upper part of the spring stream), extended areas were covered by laterally merged pustules of *Oocardium* calcite (Fig. 7A). At their surface, the initial calcification of the pustules consisted of a dense array of crystallites bounded by surfaces of the calcite rhombohedron
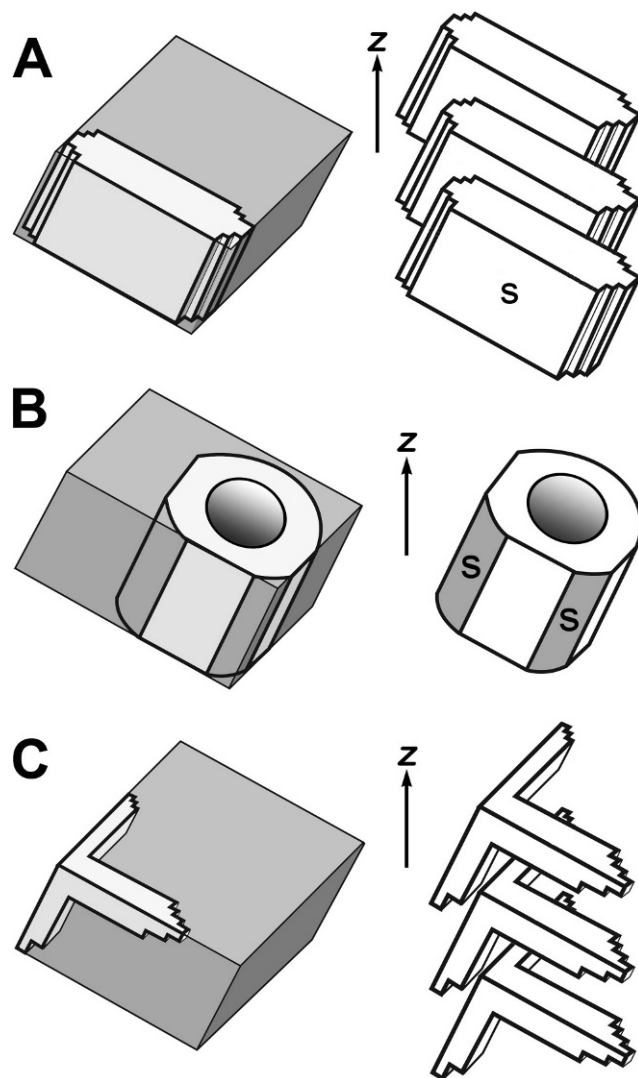

FIG. 8. Calcite rhombohedra (shown in grey), with the initial crystallization elements of Oocardium stratum for calcification types 2 (A), 3 (B), and Spiazzi (C). The arrow (z) shows the orientation of Oocardium colony growth. Surfaces labeled S consist of numerous tiny steps bound by rhombohedral surfaces.

(rhombohedral surfaces that delimit the crystallites, from a few to ~10 μm wide (Fig. 7B, C). The orientation of the rhombohedral upper surfaces was highly uniform with respect to the upward growth axis of *Oocardium*, indicating that all crystallites share identical optical orientations (Fig. 8A). The length of the crystallites subparallel to the *Oocardium* growth axis was poorly defined (Fig. 7C). The elongate shape of *discrete* crystallites (white arrows in Fig. 7C) indicates that the numerous rhombohedral surfaces originated as single crystallites or as upward-growing outliers from a larger calcite crystal underneath. However, all crystallites were bound by the same
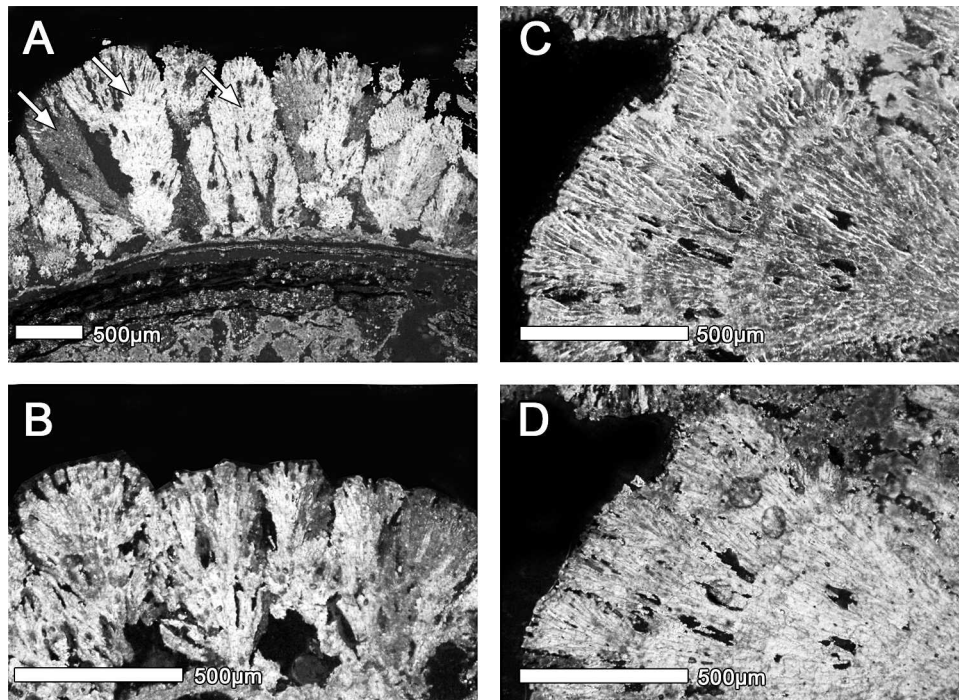
FIG. 9.   Hochtalalm calcification type 2 petrographic thin sections from station 1 (A, B where B is a close-up of A) showing deposit on phytoclast, and related close-ups of thin sections with crossed nicols (C) and dark field of crossed nicols only (D). Arrows in A indicate examples of clonal growth-related crystallization.

calcite rhombohedron surfaces. Petrographic thin sections of the pustular *Oocardium* calcite (Fig. 9A–D) indicated that the individual initial crystallites formed part of larger spar crystals.

Calcification type 3.—At H2 (lower part of spring stream) and at L, the initial crystallization proceeded by precipitation of spar-sized crystals of rhombohedral low-magnesian calcite (Figs 8B, 10A–C). This pattern indicated relatively slow calcite growth leading to fully developed calcite rhombohedron surfaces or initial crystallization as rhombohedral calcite. Some of the *Oocardium* tubes showed inward-projecting, acute dihedra (white arrows in Fig. 10B), which probably resulted from calcite crystal twinning. In thin section, type 3 initial calcification was characterized by large spar crystals containing numerous small tubes caused by upward growth of the *Oocardium* with its associated mucilage stalks (Fig. 11A, B). In turn, tubes left by the mucilage stalks may later become filled by calcite.

The special case (Spiazzi)

The tooth-like *Oocardium* calcites at S differed ultra-structurally in CP SEM (Fig. 12A). The tooth-like calcifications usually had a plane surface riddled with densely packed cells (Fig. 12A, B), but arborescent calcification prevailed within inward-projecting concave

recesses (Fig. 12C, D). On the plane surfaces, the absence of striae, grooves, or other traces of physical erosion indicated that these calcite crystals were growing. In the recesses, the surface of the initial calcification of the arborescent *Oocardium* calcite consisted of numerous rhombohedral calcite crystal skeletons (Figs 8C, 12D). Similar changes from pustular, relatively compact calcite to arborescent calcification have been seen in the recesses at T (Sanders and Rott 2009).

The sparitic crystallization elements of type 2, type 3, and the Spiazzi case

In the ditrigonal-scalenohedral crystallographic class of calcite, different sets of surfaces can result in a rhombohedron. No reference is made to specific sets of surfaces in Fig. 8A–C. All illustrated initial crystallization types (Fig. 8A–C) result in the typical coarse-sparry, arborescent fabric of *Oocardium* calcite. Initial crystallites of type Spiazzi (Fig. 8C, 12D) show a constant crystallographic orientation to each other, and to the upward-directed growth of *Oocardium*, as suggested by SEM. In Fig. 8B, a tube of *Oocardium* calcite is delimited by rhombohedron surfaces.

Initial precipitation of rhombohedral low-magnesian calcite in the immediate vicinity of viable *O. stratum* cells underwent early maturation by further,
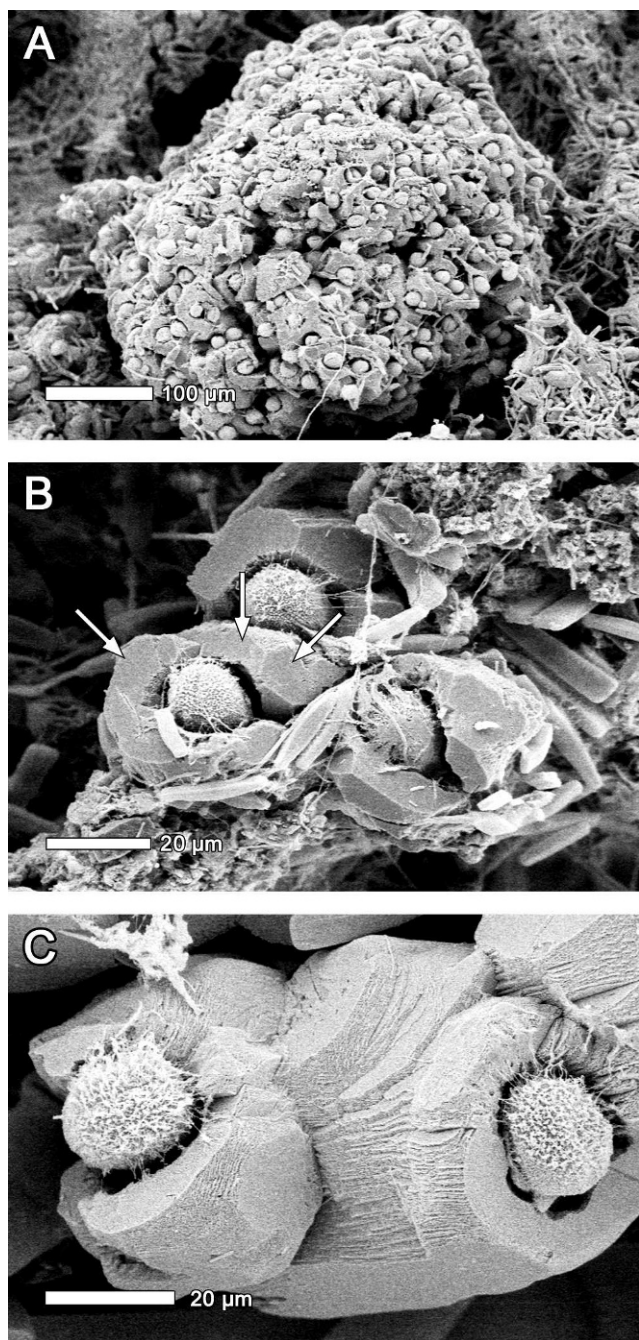
FIG. 10. Calcification type 3 from Hochtalalm 2 (lower station) (A, B) and Lingenau 2 (C). All aspects obtained with critical-point drying and scanning electron microscopy. Arrows in B indicate acute dihedral angles caused by twinning of calcite crystals.
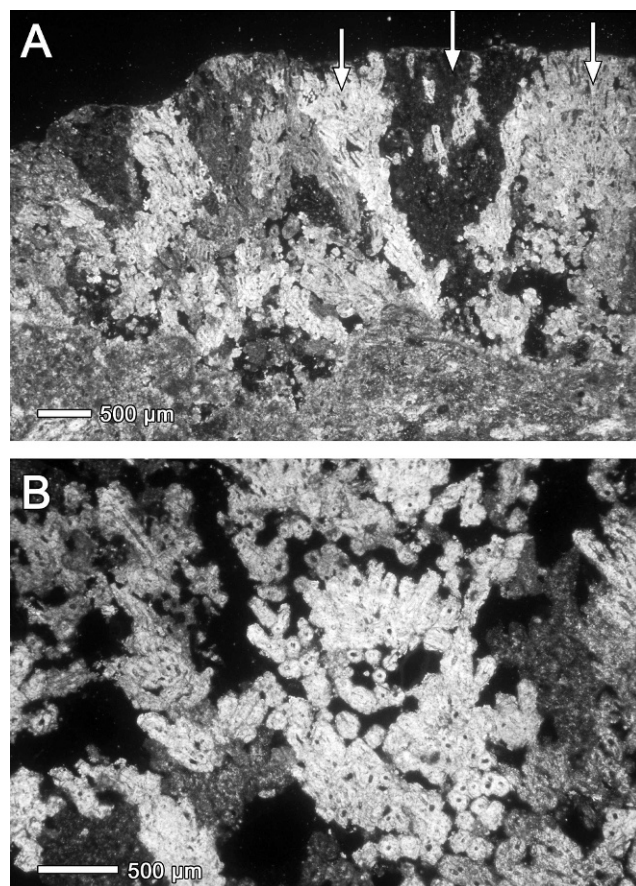

FIG. 11. Mineralogical thin section of calcification type 3 from Lingenau of a radial cross section of algal microreef showing clonal-growth-related crystal differentiations with crossed nicols (A) and close up of a near-tangential section (B). Note tubular perforations in A and B. Arrows in A indicate examples of crystals.

limited abiotic crystallization. The *Oocardium* calcite was characterized by large sparitic crystals of diagnostic arborescent structure. At sites of strong water flow (e.g., small waterfalls or water threads), the intrinsic structure was modified by recrystallization of the *Oocardium* calcite combined with abiotic $CaCO_3$

precipitation, resulting in patches of dense, translucent, coarse-sparry *combispar* with scattered relicts of the original *Oocardium*-calcite fabric.

Discussion

Our results show that consistent observations of *Oocardium* calcification can be derived from field data, but more samples and time series are needed to reveal causal relationships between initial water chemistry, features of the aquifers, and final calcite deposition types in springs. Therefore, the subsequent discussion follows from environmental and taxon-related aspects to lithological imprints and potential interrelationships and to future work on the topic.

Habitat and trait

The observed niche conditions (depressed pH, CO_2 supersaturation, gradual CO_2 degassing, and reduction
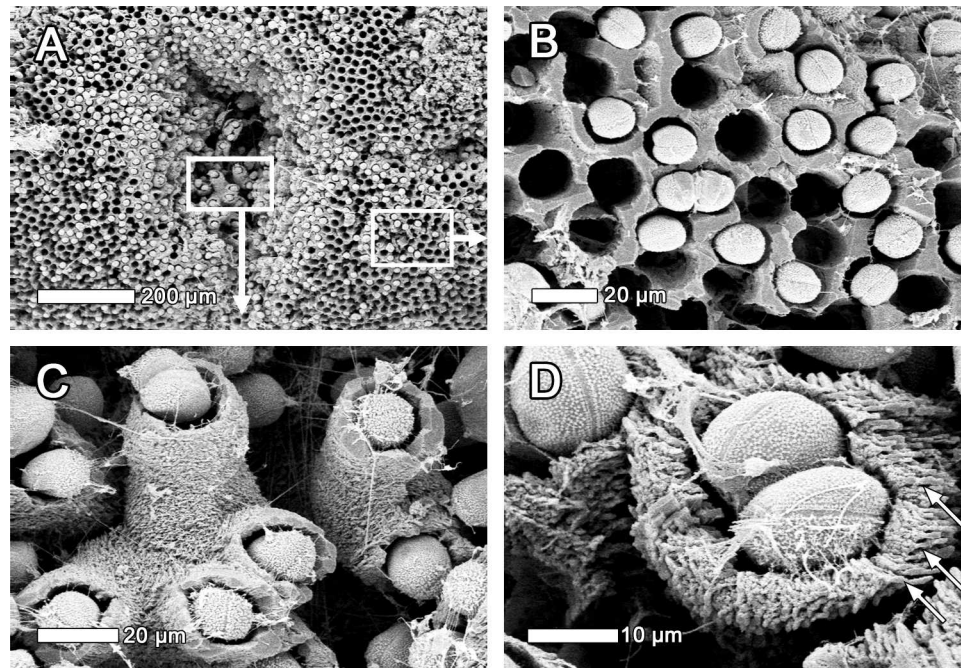
FIG. 12. Specific Spiazzi calcification type (all obtained with critical-point drying and scanning electron microscopy) in overview with eroded surface (A), detail (B), and complete calcification in depression with details (C, D). Arrows in D indicate the polygonal deposition as in Fig. 8C.

of both alkalinity and conductivity) confirm the necessity of a particular environment for active calcification (cf. Merz-Preiss and Riding 1999). The locations of most extensive *Oocardium* niches confirm earlier findings that biogenic processes for calcification linked to algal photosynthetic activity prevail in lower segments of the spring streams where pCO_2 equilibrium with the atmosphere has largely been reached (Golubić et al. 2008, Merz-Preiss and Riding 1999). In addition to aquatic bryophytes that generate the macro-architecture of SAL deposits, microbial (algal) reef formation by *Oocardium* can be spatially separated and structurally differentiated from other types of precipitation (Freytet and Verrecchia 1998). The inverse relationship between free CO_2 concentrations and *Oocardium*-related deposition rates in the upper part of spring streams may indicate that *Oocardium* is inferior to bryophytes in CO_2 uptake or incapable of taking up CO_2 at all. *Oocardium* may require carboxy-anhydrases to facilitate C acquisition for photosynthesis. In addition, calcification in moss stands does not hinder their growth.

Water-chemistry factors that impede calcification include excess reactive PO_4^{3-} (cf. Rott 1991), which was not detected in our study, although high NO_3^- (Table 2) caused by manuring in the catchment did not show an effect on calcification intensity at L. Further enhancement of nutrient fluxes at L could possibly cause outcompetition of *Oocardium* by *Vaucheria*, which was found as dominant calcifier in neighboring polluted streams (fig. 4B in Sanders et al. 2010). The highest *Oocardium* limestone deposition rate and the fastest documented calcification rate (Sanders and Rott 2009) were at L, where pCO_2 was highest (Table 2). Therefore, the degree of CO_2 supersaturation may be an indicator of the chemical disequilibrium at the spring origin, potentially related to the annual rate of limestone deposition. However, this situation would hold true only if sufficient Ca^{2+} were present to sustain $CaCO_3$ precipitation.

In permanent rheocrenes, seasonal variation in *Oocardium* growth and water temperature may influence the rate of initial calcification (Sanders and Rott 2009) and probably the diagenetic maturation into final *Oocardium* calcite fabrics (Golubić et al. 2008). However, at T, viable green, healthy-looking *Oocardium* grains are present almost year-round, whereas a maximum growth/optimum niche for green algae would be expected when light availability and temperatures are highest. Other calcite-precipitating taxa seem to have limited periods of optimum growth (*Rivularia*: spring and autumn; Rott et al. 2000).

Oocardium is the only taxon within the desmids (Zygnemaphyceae) that produces exoskeletons or algal microreefs (Pentecost 2005, Golubić et al. 2008).

Oocardium has been known for a long time but is rarely reported. It is considered an exclusively lotic benthic taxon (Hynes 1970, Whitton 1975) adapted to growth at high flow velocities (2.2–3.5 m/s; Golubić and Marcenko 1958). The specific lateral positioning of the sphenoid cells within mucilage tubes stabilized by apical master holdfasts (see Rott et al. 2010) may contribute to its adaptation to extreme lotic habitats. *Oocardium* has never been reported as noncalcified, and in contrast to the facultative calcification of most cyanobacteria, it probably is an obligate biocalcifier.

Habitat responses reflected by variability of lithological imprints

With the exception of H2 and L, *Oocardium* calcite crystallization starts with skeletons of rhombohedral low-magnesian calcite. As crystallization proceeds, the typical tubes of solid (nonporous), single-crystal calcite form a few micrometers from the top of the *Oocardium* calcite tubes. Crystallization of rhombohedral low-magnesian calcite is likely to be related to the relatively slow growth of the crystals, which allows time for fully developed crystal surfaces of the calcite rhombohedron to form.

The arborescent growth of *Oocardium* at L (Fig. 4C) seems to be uncommon and confined to specific niches or habitats. The initial crystallization of *Oocardium*-calcite tubes as crystal skeletons of rhombohedral calcite was best-developed at S. This initial process is typical for disequilibrium crystallization under marked physicochemical gradients (Sunagawa 2005), although such gradients are not related only to spring-water chemistry. For instance, in speleothem (cave) calcites, crystal skeletons and dendrites form at sites with large seasonal variations in water availability (including desiccation of sites), water discharge, or temperature (Frisia 2003, Fairchild et al. 2007). In the case of our spring-associated habitats, purely physical, seasonal fluctuations of water chemistry, water availability, or temperature may be amplified by *Oocardium* photosynthesis. More comparative data and more detailed records of variation in spring-water chemistry and physical variables are needed to understand better the formation of crystal skeletons in initial *Oocardium* calcification.

Results of statistical tests confirmed the distinctness of the 3 calcification types (Table 4). The most striking differences seem to be related to environmental factors at the spring origin because calcification types 1 and 2 differed significantly ($p < 0.05$) with pH at origin, TP, total dissolved N, temperature, and altitude. No other statistically significant differences were found.

With the possible exception of the micritic crystallites at P, the initial calcification induced in the immediate vicinity of viable *O. stratum* cells undergoes early maturation by abiotic crystallization (Sanders and Rott 2009). Previous investigations into the *Oocardium* calcites of L and T and our current observations strongly suggest that diagenetic maturation proceeds by abiotic crystallization templated by the initial *Oocardium* calcite crystals. Despite the relatively wide variability of initial calcification, the final calcite fabrics are similar, resulting in typical large, sparitic, branched *Oocardium* calcite crystals with uniform optical extinction in thin section. The extent of abiotic crystallization probably is related to both water chemistry and water supply. At L, patches of glassy, highly indurated, low-porosity, sparitic calcite (similar to cave flowstone in appearance) are formed below small waterfalls or waterthreads by intense abiotic crystallization combined with recrystallization on initial *Oocardium* calcite. The origin of this combispar texture (Sanders and Rott 2009) is revealed by traces of *Oocardium* calcite. Similar diagenetic maturation of *Oocardium* calcite has been observed by Golubić et al. (1993, 2008). Because the process is not simply recrystallization, with negligible change in total crystal volume, but is associated with significant additional spar precipitation, we propose the term combispar (recrystallization **combi**ned with further precipitation of calcite **spar**) for such materials.

Literature Cited

CANTONATI, M., E. BERTUZZI, A. SCALFI, AND V. CAMPANA. 2009. The potential importance for spring conservation of residual habitats after flow capturing: a case study. Verhandlungen der Internationalen Vereinigung für theoretische und angewandte Limnologie 30:1267–1270.

CANTONATI, M., E. ROTT, D. SPITALE, N. ANGELI, AND J. KOMÁREK. 2012. Are benthic algae related to spring types? Freshwater Science 31:481–498.

EU HD (EUROPEAN UNION HABITAT DIRECTIVE). 1992. European Commission, Environment Directorate-General: Council Directive 92/43/EEC of 21 May 1992 on the conservation of natural habitats and of wild fauna and flora. Official Journal of the European Union L 206:7–50.

FAIRCHILD, I. J., S. FRISIA, A. BORSATO, AND A. F. TOOTH. 2007. Speleothems. Pages 200–245 *in* D. J. Nash and S. J. McLaren (editors). Geochemical sediments and landscapes. Blackwell, Oxford, UK.

FORD, T. D., AND H. M. PEDLEY. 1996. A review of tufa and travertine deposits of the world. Earth Science Reviews 41:117–175.

FREYTET, P., AND E. P. VERRECCHIA. 1998. Freshwater organisms that build stromatolites: a synopsis of biocrystallization by prokaryotic and eukaryotic algae. Sedimentology 45:535–563.

FRISIA, S. 2003. Le tessiture negli speleotemi. Studi Trentini di Scienze Naturali – Acta Geologica 80:85–94.

GERSTBERGER, P., AND P. LEINS. 1978. Rasterelektronenmikroskopische Untersuchungen an Blütenknospen von *Physalis philadelphica* (Solanaceae). Anwendung einer neuen Präparationsmethode. Berichte der Deutschen Botanischen Gesellschaft 91:381–387.

GOLUBIĆ, S., AND E. MARCENKO. 1958. Zur Morphologie und Taxonomie der Desmidiaceengattung *Oocardium*. Aquatic Sciences: Research Across Boundaries 20:177–185.

GOLUBIĆ, S., C. VIOLANTE, V. FERRERI, AND B. D'ARGENIO. 1993. Algal control and early diagenesis in Quaternary travertine formation (Rocchetta a Volturno, Central Appenines). Pages 231–247 *in* F. Brattolo, P. De Castro, and M. Parente (editors). Studies on fossil benthic algae. Bollettino della' Societa Paleontologica Italiana Special Volume 1.

GOLUBIĆ, S., C. VIOLANTE, A. PLENKOVIĆ-MORAJ, AND T. GRGASOVIĆ. 2008. Travertines and calcareous tufa: an insight into diagenesis. Geologia Croatica 61:363–378.

HÜTTER, L. 1994. Wasser und Wasseruntersuchung. 6th edition. Laborbücher Salle und Sauerländer, Frankfurt am Main, Germany.

HYNES, H. B. N. 1970. The ecology of running waters. Liverpool University Press, Liverpool, UK.

MACKERETH, F. J. H., J. HERON, AND J. TALLING. 1978. Water analysis: some revised methods for limnologists. Scientific Publications 36. Freshwater Biological Association, Cumbria, UK.

MANN, H. B., AND D. R. WHITNEY. 1947. On a test of whether one of two random variables is stochastically larger than the other. Annals of Mathematical Statistics 18:50–60.

MERZ-PREISS, M., AND R. RIDING. 1999. Cyanobacterial tufa calcification in two freshwater streams: ambient environment, chemical thresholds and biological processes. Sedimentary Geology 126:103–124.

OBENLÜNESCHLOSS, J., AND J. SCHNEIDER. 1991. Ecology and calcification patterns of *Rivularia* (Cyanobacteria). Algological Studies 64:489–502.

PEDLEY, M. 2009. Tufas and travertines of the Mediterranean region: a testing ground for freshwater carbonate concepts and developments. Sedimentology 56:221–246.

PENTECOST, A. 1987. Growth and calcification of the freshwater cyanobacterium *Rivularia haematites*. Proceedings of the Royal Society of London Series B: Biological Sciences 232:125–136.

PENTECOST, A. 1991. A new and interesting site for calcite-encrusted desmid *Oocardium stratum* Nägeli in the British Isles. British Phycological Journal 26:297–301.

PENTECOST, A. 2005. Travertine. Springer, Berlin, Germany.

RIETH, A. 1970. Süßwasser-Algenarten in Einzeldarstellung II. *Oocardium stratum* nach Material aus Kuba. Kulturpflanze 18:51–71.

ROTT, E. 1991. Oncoids from the summer-warm River Alz (Bavaria): morphology and dominant cyanophytes. Algological Studies 64:469–482.

ROTT, E., A. HOLZINGER, D. GESIERICH, W. KOFLER, AND D. SANDERS. 2010. Cell morphology, ultrastructure and calcification pattern of *Oocardium stratum*, a peculiar lotic desmid. Protoplasma 243:39–50.

ROTT, E., L. WALSER, AND M. KEGELE. 2000. Ecophysiological aspects of macroalgal seasonality in a gravel stream in the Alps (River Isar, Austria). Verhandlungen der Internationalen Vereinigung für theoretische und angewandte Limnologie 27:1622–1625.

SANDERS, D., AND E. ROTT. 2009. Contrasting styles of calcification by the micro-alga *Oocardium stratum* Nägeli 1849 (Zygnematophyceae) in two limestone-precipitating springs of the Alps. Austrian Journal of Earth Sciences 102:34–49.

SANDERS, D., W. WERTL, AND E. ROTT. 2010. Spring-associated limestones of the Eastern Alps: overview of facies, deposystems, minerals and biota. Facies 57:395–416.

SCHNEIDER, J., H. G. SCHRÖDER, AND T. LE CAMPION-ALSUMARD. 1983. Algal micro-reefs: coated grains from freshwater environments. Pages 284–298 *in* T. M. Peryt (editor). Coated grains. Springer Berlin, Heidelberg, Germany.

SUNAGAWA, I. 2005. Crystals. Growth, morphology and perfection. Cambridge University Press, Cambridge, UK.

TSCHAIKNER, A., G. GÄRTNER, AND W. KOFLER. 2008. *Coelastrella aeroterrestrica* sp. nov. (Chlorophyta, Scenedesmoideaea)—a new, obviously often overlooked aeroterrestrial species. Algological Studies 128:11–20.

WALLNER, J. 1933. *Oocardium stratum* Naeg., eine wichtige tuffbildende Alge Südbayerns. Planta 20:287–293.

WALLNER, J. 1934a. Über die Beteiligung kalkablagernder Pflanzen bei der Bildung südbayerischer Tuffe. Bibliotheca Botanica 110:1–30.

WALLNER, J. 1934b. Über die Verbreitungsökologie der Desmidiacee *Oocardium*. Planta 23:249–263.

WALLNER, J. 1935. Zur Kenntnis der Gattung *Oocardium*. Hedwigia 75:130–136.

WETZEL, R. G. 1975. Limnology. Saunders, Philadelphia, Pennsylvania.

WHITTON, B. A. 1975. Algae. Pages 81–105 *in* B. A. Whitton (editor). Blackwell Studies in Ecology. Blackwell, Oxford, UK.